Journal of Cranio-Maxillo-Facial Surgery 44 (2016) 215–223

Contents lists available at ScienceDirect

Journal of Cranio-Maxillo-Facial Surgery

journal homepage: www.jcmfs.com

Mandibular angle split osteotomy based on a novel augmented reality navigation using specialized robot-assisted arms—A feasibility study

Li Lin [a, 1], Yunyong Shi [b, 1], Andy Tan [a], Melia Bogari [a], Ming Zhu [a], Yu Xin [a], Haisong Xu [a], Yan Zhang [a, ***], Le Xie [b, c, **], Gang Chai [a, *]

[a] Department of Plastic and Reconstructive Surgery, Shanghai 9th People's Hospital, Shanghai Jiao Tong University School of Medicine, 639 Zhi Zao Ju Rd, Shanghai, 200011, China
[b] School of Biomedical Engineering, Shanghai Jiao Tong University, China
[c] National Digital Manufacturing Technology Center, Shanghai Jiao Tong University, China

ARTICLE INFO

Article history:
Paper received 18 July 2015
Accepted 20 October 2015
Available online 14 November 2015

Keywords:
Augmented reality
Mandibular angle split osteotomy
Robot-assisted surgery
Computer-assisted surgery

ABSTRACT

Purpose: Augmented reality (AR) navigation, is a visible 3-dimensional display technology, that, when combined with robot-assisted surgery (RAS), allows precision and automation in operational procedures. In this study, we used an innovative, minimally invasive, simplified operative method to position the landmarks and specialized robot-assisted arms to apply in a rapid protyping (RP) model. This is the first report of the use of AR and RAS technology in craniomaxillofacial surgery.
Method: Five patients with prominent mandibular angle were randomly chosen for this feasibility study. We reconstructed the mandibular modules and created preoperational plans as semi-embedded and nail-fixation modules for an easy registration procedure. The left side of the mandibular modules comprised the experimental groups with use of a robot, and the right sides comprised the control groups without a robot. With AR Toolkits program tracking and display system applied, we carried out the operative plans and measured the error.
Results: Both groups were successfully treated in this study, but the RAS was more accurate and stable. The average position and angle were significant ($p < 0.01$) between the 2 groups.
Conclusions: This study reports a novel augmented reality navigation with specialized robot-assisted arms for mandibular angle split osteotomy. AR and RAS can be helpful for patients undergoing craniomaxillofacial surgery.

1. Introduction

Mandibular angle split osteotomy (MASO) is widely used in treating prominent mandibular angle and aims to improve cosmetic results in the patients. Surgeons have conventionally performed this procedure based on computed tomography (CT) images and clinical experience. The most difficult aspects of MASO are the complexity of the anatomical structure and the narrow field of view allowed by an intraoral incision (Hong et al., 2014). The advantages of augmented reality (AR) are the ability to provide direct perception of the position of crucial structures and to assist surgeons in developing preoperational plans; which make AR an excellent solution to problems frequently encountered with MASO.

Augmented reality (AR), which is developed by computer technology, can combine reality and digital information. The major characteristic of augmented reality, which enhances the sensation of the user, are a combination of virtual reality, real-time interaction, and 3-dimensional display (Berryman, 2012). With the advent of computed tomography (CT), magnetic resonance imaging (MRI), and digital radiography, there is the possibility of creating virtual

* Corresponding author. Department of Plastic and Reconstructive Surgery, Shanghai 9th People's Hospital, Shanghai Jiao Tong University School of Medicine, 639 Zhi Zao Ju Rd, Shanghai, 200011, China.
** Corresponding author. School of Biomedical Engineering, Shanghai Jiao Tong University, China and National Digital Manufacturing Technology Center, Shanghai Jiao Tong University, China.
*** Corresponding author.
E-mail addresses: 13651817522@163.com (Y. Zhang), lexie@sjtu.edu.cn (L. Xie), 13918218178@163.com (G. Chai).
[1] Li Lin and Yunyong Shi contributed equally to this paper.

http://dx.doi.org/10.1016/j.jcms.2015.10.024
1010-5182/

data to provide information for navigation systems in medical areas such as neurosurgery (Cabrilo et al., 2014), orthopedics (Zemirline et al., 2013), maxillofacial surgery (Qu et al., 2014), urology (Hughes-Hallett et al., 2014), gastrointestinal surgery (Marzano et al., 2013), pediatric surgery (Souzaki et al., 2013), and cardiology (Szabo et al., 2013), among other areas. Even though many different kinds of AR systems have been used in studies, no simple registration and minimally invasive method have been reported.

Use of medical robots may result in decreased hospitalization time, lower complication rates, less postoperative pain, and faster recovery (Pugin et al., 2011). Moreover, medical robots can also reduce tremble and fatigue in the surgeon. In the past decades, there have been many applications in areas of plastic surgery (Selber, 2014). However, considering the high cost, necessity of long-term training, and uncertain security, there is no specialized robot that is widely used in craniomaxillofacial surgery.

We chose MASO for our study because of the simplicity of the procedure. In this study, we aimed to use an innovative, minimally invasive, simplified operative method to position the landmarks for the AR system, along with specialized robot-assisted arms to apply in a rapid prototyping (RP) model. Such a method, which combines the advantages of both AR and RAS technology, is a novel approach in craniomaxillofacial surgery. By combining AR and RAS technology, we can find a new way to perform more complicated surgery, entering into a new era of intelligence, visualization, and automation for craniomaxillofacial surgery.

2. Material and methods

2.1. Model resource

Five patients with mandibular angle prominence were randomly chosen from an image work station in our department between 2011 and 2014. By reading the digital imaging and communications in medicine (DICOM) data for computed tomography (Brilliance 64 slice spiral CT, Philips, the Netherlands), the information was input in our software station (Materialise, Ann Arbor, Michigan, USA). We set a threshold value to distract bone and soft tissues for their different densities and reconstructed a 3-dimensional skull image, using rapid prototyping (RP) technology (ProJet 660 Pro, 3DSYSTEM, USA) models that were readily available.

2.2. Preoperational design

The most common complication of MASO is nerve damage after surgery. To prevent this problem, the first step was to mark the mandibular branch of the facial nerve. To ensure the section plane, we selected 6 key points, based on clinical experience, for achieving cosmetic results without damaging the nerve and to maintain a safe distance during the operation.

By using RAS technology, we performed a drilling method as a means of transitioning to automatic MASO. In theory, numerous hole paths can be used to create a cutting plane, and with the force-control device of robot-assisted arms, the finishing drilling point must stop at the bone part as well as plan. For a better perception of the AR, we also added a virtual model of a drill for better viewing of the navigation system (2-mm-diameter drills, GD456M, Aesculap, Germany) (Fig. 1).

2.3. Mark complex

In this study, we created a new method by computer-assisted design (CAD) software to make a semi-embedded and nail-fixation mark complex (MC). The first step in making a fixation module involved drilling 3 holes 3–4 mm in thickness for screws. As a result, there was no extra damage to the patient because the fixation part was cut as planned. Then, we designed a delicate and custom-made module connector that attached to the mark module. These 3 parts comprised the mark complex (MC). Finally, we output the MC data as an STL file with computer-aided manufacturing (CAM) technology to create an actual model (Fig. 2).

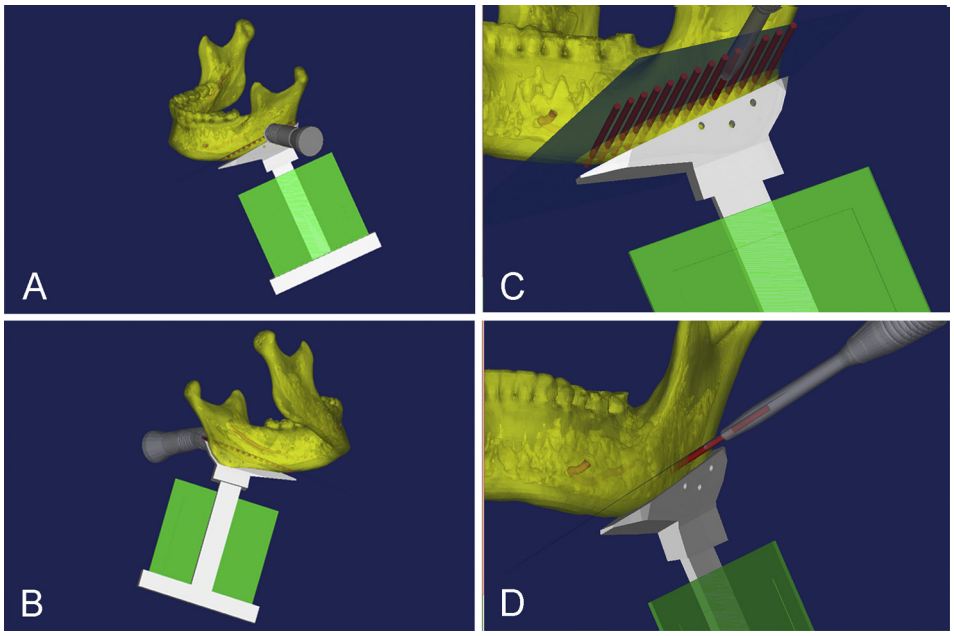

Fig. 1. Preoperational design. (A) Anterior portion of the preoperational design. (B) Posterior portion of the preoperational design. (C) Perspective of the preoperational design. (D) Single path of the preoperational design. Yellow: mandible; blue: cutting plane; light red: nerve; dark red: drilling path; white: mark complex; green: mark simulation; gray: drill simulation.

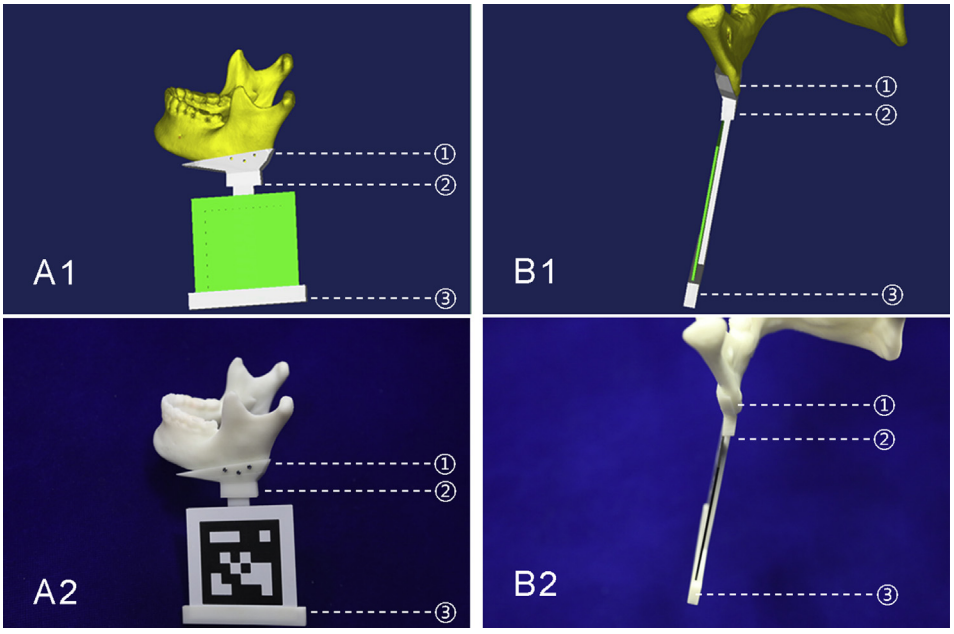

Fig. 2. Mark complex. (A1) Anterior portion of the preoperational design. (A2) Anterior portion of the actual model. (B1) Lateral portion of the preoperational design. (B2) Lateral portion of the actual model. (①) Fixation module. (②) Connected module. (③) Mark module.

For better results, we designed a simplified connection module, which was more complex in clinical applications. The mark module was manufactured and standardized so that there was no system error for the position of the mark.

2.4. AR system

2.4.1. Operational system

The display software that we used is based on AR Toolkits. This is open-source software that can be easily used to recognize the MC and to adjust the parameters of the 3-dimensional material so that the virtual images can be adjusted in the AR Toolkits system. In an earlier study, we created a simulation template for actual mark positions for resetting the coordinates of the virtual images by reference to the central point (Fig. 3) of the mark, so it is easy to register virtual plans with actual positions.

2.4.2. Tracking system

MicronTracker (Claron Company, Canada) is the first system to be developed with 3-dimensional vision and tracking functions. This device detects and calculates the space location through the probe, which has optical sensors with 3 cameras to merge 3-

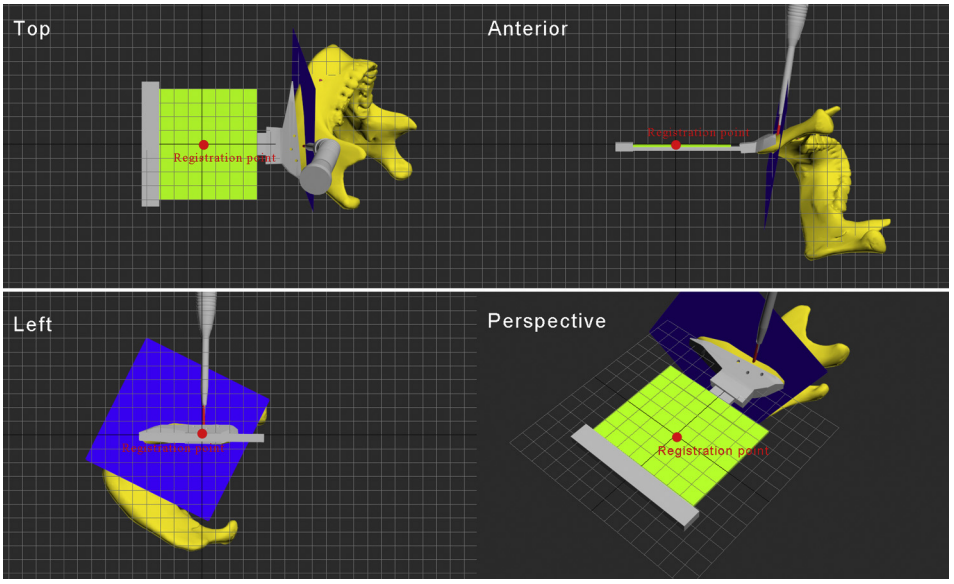

Fig. 3. Registration system. At our image work station, we have developed this template registration program by reference of the central point in 3-dimensional positions of the real mark in our earlier study. The AR system's original coordinates are based on the central point of the mark as well as the tracking system, so it is easy to register the mark simulation to the real position.

dimensional images for the surgeon. The advantage of this is the use of stereoscopic vision in real time to detect and to track specially marked objects and thereby avoid 2-dimensional and 3-dimensional display errors (Fig. 4A).

2.4.3. Display system

nVisor ST60 (NVIS Company, USA) is one kind of helmet-mounted display (HMD) for showing 3-dimensional virtual images with the assistance of a tracking system. The image information is sent from the computer to this device, and the 3-dimensional images are shown at the glass directly in front of the eyes, so there is no need to switch the vision field from the monitor to the operation side (Fig. 4C).

Fig. 5A and B was screen captured by the computer, which displayed only 2-dimensional images of the preoperational design for the X and Y dimensions. Thus there is some display error in the pictures, especially in regard to the distance part, but this has resolved on the HMD screen in its 3-dimensional display. Drill simulation is somewhat apart from the activation of the operative process, so the key point of AR navigation is the alignment of the real drill with the drilling path.

2.4.4. RAS system

The robot has 7 degrees of freedom. The structure of the surgical robot consists mainly of the following parts: support module, position control module, attitude control module, motor motion module, and surgical operation module. The whole robot-assisted device is manufactured from an aluminum alloy to guarantee strength and stiffness, which can effectively ease the weight of the device (Fig. 6A).

In the surgical operation module of the robotic device, the pressure sensor is fixed through the fixture. When the fixture makes contact, the pressure sensor generates voltage under pressure, and the data acquisition card is used to detect the value of the pressure in real time to determine the drilling process.

In the motor control of the robot, the traditional Proportion Integration Differentiation (PID) controller will produce a large error in the process of control. To resolve this problem, the control method adopts fuzzy control (Fig. 6B).

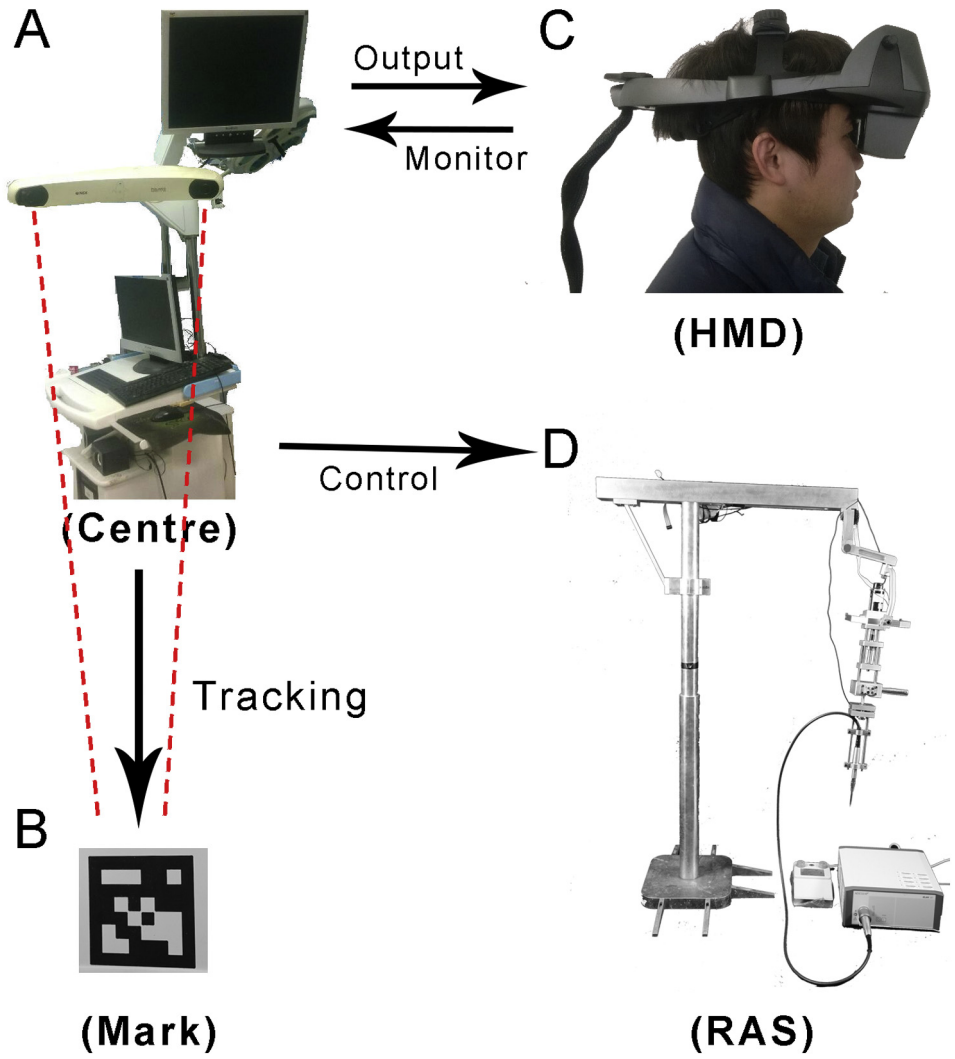

Fig. 4. Structure of the AR system. (A) MicronTracker and AR Toolkits system. (B) Marker system. (C) HMD system. (D) RAS system. MicronTracker detects and tracks the marker position in real time while the virtual image information is picked up. The information is then input into the AR Toolkits system at the computer work station and output to the HMD system. In the meantime, the real environment information is also collected by the cameras of MicronTracker. With a combination of 3 directions of information, the AR Toolkits system will reconstruct 3-dimensional images and show them in HMD. With virtual and actual images merged, surgeons perform the operations with the assurance of the starting position of the drill of the RAS system by monitoring the HMD without switching to the computer screen.

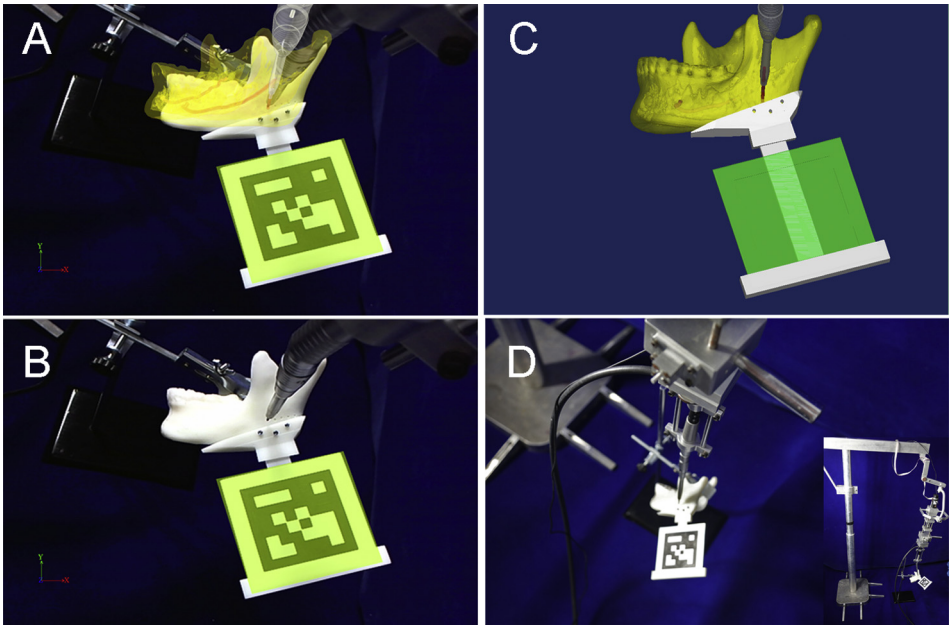

Fig. 5. Operation process. (A) Drill position with AR navigation. (B) Drill position in reality. (C) Drill position of preoperational design. (D) Position for operation. Yellow: mandible; light red: nerve; dark red: drilling path; green: mark simulation; gray: drill simulation.

The surgical robot control program uses VC++ programming language; the data appear through a user interface, the actual measured force at time N and N+1 are compared. Potential breakthrough is detected through a change in resistance to judge whether the drill will break-through the bone; when the value is biased toward negative deviation, the maximum bone density has been reached; when the value is zero, the bone is penetrated. If the pressure wave appears twice, the robot has completed the course of drilling the bone (Fig. 6C).

2.4.5. Accuracy measurement

To contrast the AR and RAS systems, we use the left side of module with the RAS system as the experimental group, and the right side of the module without the RAS system as a control group.

The MicronTracker can provide virtual position and angle information as well as the actual ones. We selected 4 point groups for each case to detect the start and finish center-of-drilling paths at the start (Fig. 7A) and finish (Fig. 7B) points in reality and in virtual reality. Each group has 2 points with 3-dimensional coordinate values for both reality and virtual reality so that the deviation of position and angle can be calculated. Data are analyzed using a *t*-test to obtain statistically significant results of this method for 5 cases.

The coordinate value detected by MicronTracker is matrix data that can be converted to numeric data and given as millimeters. The position error can be calculated by a formula by coordinate values as 3-dimensional data for both virtual reality and reality. There is an intersection angle for the virtual reality and reality lines, such as aa′, which can be considered the angle error for the system. Using a vector calculus method, this angle error can be measured.

3. Results

The AR and RAS systems were applied in this study. Each module was used for 15 min for 10–20 drilling processes. Four groups of points used as drilling paths were chosen for statistical purposes.

The position error was 0.95 ± 0.14 mm (Table 1a) in the experimental group and 1.64 ± 0.57 mm (Table 1b) in the control group, with a significant difference ($p < 0.01$). The average angle error was 5.34 ± 2.48° (Table 2a) in the experimental group and 10.46 ± 3.46° (Table 2b) in the control group, with a significant difference ($p < 0.01$).

4. Discussion

To achieve a more esthetic appearance in Asian women, MASO is often used to treat patients with broad or squarish faces. Since the first mandibular angle osteotomy was reported in craniomaxillofacial surgery, researchers and surgeons have tried to find an easily operated and time-saving method. However, 2 major disadvantage of classical MASO have been observed: the first is the possibility of condyle fracture, and the second is the possibility of nerve damage in clinical practice (Deguchi et al., 1997). To prevent these damages from occurring, various modifications have been made (Park et al., 2014). The conventional extraoral approach of oblique ostectomy is easily carried out but leaves a scar after surgery and may leave an unsatisfactory mandibular curve. The intraoral method is less invasive, but the risks are accidental mandibular fracture, unsatisfactory contour, and damage to the nerve (Yang et al., 2009). The invisibility of anatomical structures and the potential for unstable human operation become the main problems to be solved.

AR technology originated from the HMD invention in the 1960s and developed rapidly in the 1990s. Current study of AR in the medical field is focused on navigation and registration technology and can be classified into 2 groups: a marker-based system using skin markers, implanted screws or templates, and splints (Tsuji et al., 2006; Mischkowski et al., 2006; Badiali et al., 2014); and a marker-free system, using laser scanning or ultrasound (Marmulla et al., 2005; Hoffmann et al., 2005). The benefit of implanted screws is greater accuracy; the disadvantage is the invasiveness of the procedure. Due to the limited precision in soft tissue situations altered by surgical procedures, skin marker and marker-free

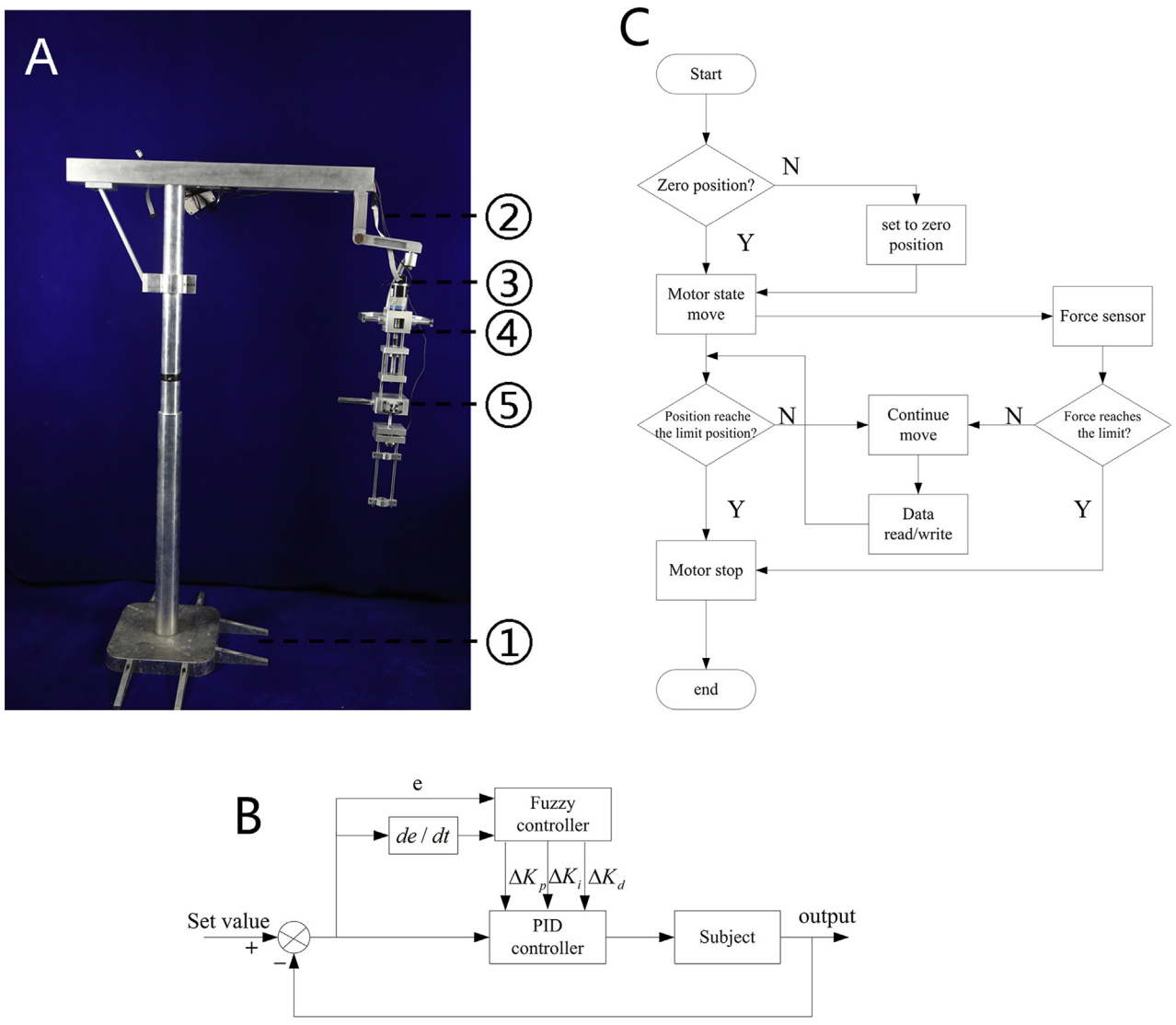

Fig. 6. Structure of the RAS. (A) Mechanical device. (①) Support module. (②) Position control module. (③) Motor motion module. (④) Attitude control module. (⑤) Surgical operation module. (B) Fuzzy PID controller. (C) Control Flow chart.

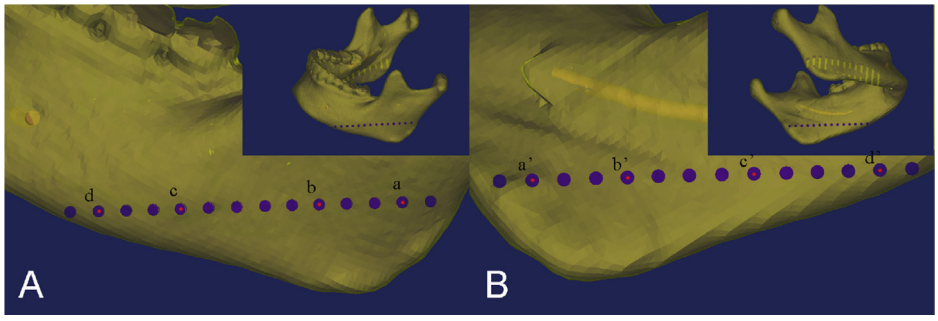

Fig. 7. Error measurement. (A) Detection points on the outside. (B) Detection points on the inside.

systems are restricted in clinical applications. Another effective method is to use an occlusal splint, which is feasible in cranio-maxillofacial surgery (Zhu et al., 2011). However, this method is complicated, with a large amount of training required for making dental casts and using different software applications. In addition, this method is not suitable for patients with tooth loosening or trauma.

Considering the minimal invasiveness, simplified operation, and limited error associated with the AR system in clinical applications, we used semi-embedded and nail-fixation MC in

Table 1a
Position error for system in the experimental group.

No. of exp. patients		Virtue			Reality			P.E. (mm)
		X1	Y1	Z1	X2	Y2	Z2	
1	a	125	71.23	171.39	125.49	71.68	171.19	0.69
	b	137.21	65.09	168.95	137.98	64.68	168.46	1.00
	c	158.69	52.38	164.06	159.15	52.79	163.57	0.79
	d	168.46	45.04	158.2	167.69	44.87	158.69	0.93
	a′	120.12	66.31	162.6	121.09	66.45	162.11	1.10
	b′	132.81	61.22	160.64	133.3	61.98	160.31	0.96
	c′	152.83	47.65	152.83	153.32	47.23	151.86	1.17
	d′	163.57	41.18	148.44	162.79	41.66	148.53	0.92
	Mean ± SD							0.94 ± 0.15
2	a	122.56	47.38	177.73	123.54	47.54	177.64	1.00
	b	130.37	42.63	176.27	130.86	43.58	176.2	1.07
	c	145.51	32.47	172.36	146.48	32.69	172.16	1.01
	d	154.3	26.22	169.92	153.34	26.45	169.9	0.99
	a′	118.16	42.33	169.37	119.14	42.54	169.87	1.12
	b′	126.95	37.42	167.43	126.18	37.26	167.68	0.83
	c′	141.11	26.35	164.55	140.62	25.89	164.93	0.77
	d′	149.9	20.04	162.6	150.08	20.58	162.24	0.67
	Mean ± SD							0.93 ± 0.16
3	a	125.98	51.19	178.71	126.77	51.44	179.2	0.96
	b	135.25	45.03	174.32	135.41	44.37	173.86	0.82
	c	152.34	35.11	165.04	153.18	35.34	164.55	1.00
	d	160.16	27.4	159.18	159.38	27.58	159.94	1.10
	a′	121.09	42.53	171.39	120.61	43.03	171.66	0.74
	b′	129.88	36.28	166.5	129.51	35.86	166.99	0.74
	c′	146	24.96	156.25	146.87	24.56	156.41	0.97
	d′	154.31	18.75	151.37	153.81	19.23	150.68	0.98
	Mean ± SD							0.92 ± 0.13
4	a	122.56	60.07	173.34	123.15	59.77	172.88	0.81
	b	130.86	53.68	172.36	131.75	54.49	172.24	1.21
	c	145.46	38.81	169.99	145.37	39.65	169.45	1.00
	d	154.3	30.12	163.57	153.81	30.85	164.24	1.11
	a′	118.65	57.63	166.02	119.54	57.29	166.34	1.01
	b′	126.46	51.22	164.06	126.78	50.47	163.57	0.95
	c′	140.62	34.89	156.74	140.14	34.13	157.51	1.18
	d′	148.93	26.15	152.83	148.44	26.98	152.34	1.08
	Mean ± SD							1.04 ± 0.13
5	a	123.02	53.72	166.02	123.72	54.31	166.39	0.99
	b	132.32	46.29	165.53	132.85	45.63	165.13	0.94
	c	149.9	33.82	164.04	149.23	33.72	164.56	0.85
	d	158.69	25.09	160.64	159.42	25.74	160.93	1.02
	a′	119.14	48.65	157.71	119.73	48.36	157.89	0.68
	b′	128.91	42.52	156.94	127.93	42.35	157.71	1.26
	c′	145.02	28.81	153.81	145.31	28.25	154.49	0.93
	d′	154.79	21.19	151.86	154.3	21.36	152.43	0.77
	Mean ± SD							0.93 ± 0.17
Total	Mean ± SD							0.95 ± 0.15

Abbreviations: No. = number; exp. = experimental group; a, b, c, d = center point of start drill; a′, b′, c′, d′ = center point of finish drill; P.E. = position error; mm = millimeter; SD = standard deviation.

Table 1b
Position error for system in the control group.

No. of ctrl. patients		Virtue			Reality			P.E. (mm)
		X1	Y1	Z1	X2	Y2	Z2	
1	a	121.09	72.47	75.2	122.07	73.72	74.71	1.66
	b	134.28	66.34	75.68	135.74	66.35	75.78	1.46
	c	150.39	56.23	78.61	149.9	57.45	78.61	1.31
	d	162.6	48.61	82.03	161.13	48.79	81.54	1.56
	a′	120.12	67.43	83.01	118.65	67.47	83.01	1.47
	b′	132.81	61.21	84.47	133.3	60.09	84.47	1.22
	c′	148.44	50.01	89.84	146.97	48.77	88.87	2.15
	d′	160.16	42.53	93.26	160.64	41.28	92.77	1.43
	Mean ± SD							1.53 ± 0.28
2	a	124.51	41.21	81.05	122.56	41.31	80.08	2.18
	b	131.84	37.46	83.98	133.79	37.54	84.96	2.18
	c	144.53	27.53	90.82	144.04	28.76	90.82	1.32
	d	152.34	22.61	93.26	153.81	24.88	93.26	2.70
	a′	120.12	37.42	87.4	119.14	36.25	86.91	1.60
	b′	127.93	33.78	89.36	126.46	32.51	90.87	2.46
	c′	139.65	22.42	97.66	140.14	23.75	98.14	1.50
	d′	146.97	17.39	100.1	146.48	17.52	99.12	1.10
	Mean ± SD							1.88 ± 0.58
3	a	117.19	50.02	74.22	116.21	48.71	73.73	1.71
	b	125.98	43.71	77.64	126.46	42.54	77.64	1.26
	c	143.07	33.78	83.5	143.07	35.08	83.5	1.30
	d	150.88	27.53	86.91	152.34	27.54	87.89	1.76
	a′	111.82	42.59	81.54	111.33	43.75	81.24	1.29
	b′	120.61	36.22	84.96	119.14	36.21	83.98	1.77
	c′	137.21	25.12	90.82	137.21	26.28	92.29	1.87
	d′	146	20.08	94.24	146.48	20.34	96.19	2.02
	Mean ± SD							1.62 ± 0.30
4	a	120.12	57.42	80.08	119.16	57.59	81.05	1.38
	b	127.93	50.12	82.03	129.39	50.04	82.03	1.46
	c	142.58	35.1	88.38	141.11	34.93	88.38	1.48
	d	149.41	26.13	91.8	150.39	27.12	91.8	1.39
	a′	116.21	56.22	89.36	117.68	56.28	88.87	1.55
	b′	124.02	47.49	91.8	122.56	47.51	91.56	1.48
	c′	137.7	32.38	99.12	138.67	32.54	100.1	1.39
	d′	145.51	25.04	102.54	144.04	25.1	101.07	2.08
	Mean ± SD							1.53 ± 0.23
5	a	143.55	55.04	58.11	144.04	53.85	58.59	1.37
	b	151.37	47.52	62.5	149.9	46.33	61.01	2.41
	c	166.99	32.61	70.8	168.46	32.41	71.78	1.78
	d	172.36	24.89	77.64	173.83	25.03	78.12	1.55
	a′	135.74	52.39	67.87	135.32	51.21	67.87	1.25
	b′	144.53	45.06	71.29	145.51	44.95	70.75	1.12
	c′	159.18	30.14	81.54	158.2	30.04	80.59	1.37
	d′	166.5	22.54	84.96	166.99	23.53	86.91	2.24
	Mean ± SD							1.64 ± 0.47
Total	Mean ± SD							1.64 ± 0.57

Abbreviations: No. = number; ctrl. = control group; a, b, c, d = center point of start drill; a′, b′, c′, d′ = center point of finish drill; P.E. = position error; mm = millimeter; SD = standard deviation.

resection part-way and combined the advantages of the different methods. With the template simulations for actual marker positions, the registration process was simplified and easily operated by the surgeons.

The modern history of robotics in surgery began with performing neurosurgical biopsies in 1985 (Kwoh et al., 1988). RAS has offered several advantages over conventional surgery, such as 3-dimensional vision, dexterity enhancement, and tremor control for the surgeon (Valero et al., 2011). On the basis of automaticity, robots fall into 3 discrete categories: passitive (completely operated by surgeons); restricted (execute simple programs, controlled for critical operations); and automatic (fully intelligent to perform surgery). For safety purposes, our robot-assisted arms with a force-control device were used only under the control of a surgeon as a restricted robotically assisted procedure.

However, there are still some aspects of our system that need to be improved for future clinical applications. For the AR system, the connection module part of MC, which as a bridge-support module, represents the most difficult design process in light of individual differences, and a curved design will more closely conform to clinical situations. For the RAS system, robot-assisted arms with fewer extra modules and smaller machine size will be easier for surgeons to operate.

5. Conclusion

In this study, novel augmented reality navigation with a specialized robot-assisted arm system for mandibular angle split osteotomy has been successfully performed, with limited errors. Computer-assisted surgery and robot-assisted surgery can be

Table 2a
Angle error for system in the experimental group.

No. of exp. patients		Virtue			Reality			A.E. (°)
		X1	Y1	Z1	X2	Y2	Z2	
1	aa′	−4.88	−4.92	−8.79	−4.4	−5.23	−9.08	3.14
	bb′	−4.4	−3.87	−8.31	−4.68	−2.7	−8.15	6.61
	cc′	−5.86	−4.73	−11.23	−5.83	−5.56	−11.71	2.74
	dd′	−4.89	−3.86	−9.76	−4.9	−3.21	−10.16	3.68
	Mean ± SD							4.04 ± 1.75
2	aa′	−4.4	−5.05	−8.36	−4.4	−5	−7.77	1.91
	bb′	−3.42	−5.21	−8.84	−4.68	−6.32	−8.52	7.79
	cc′	−4.4	−6.12	−7.81	−5.86	−6.8	−7.23	8.07
	dd′	−4.4	−6.18	−7.32	−3.26	−5.87	−7.66	6.51
	Mean ± SD							6.07 ± 2.86
3	aa′	−4.89	−8.66	−7.32	−6.16	−8.41	−7.54	5.49
	bb′	−5.37	−8.75	−7.82	−5.9	−8.51	−6.87	4.55
	cc′	−6.34	−10.15	−8.79	−6.31	−10.78	−8.14	3.48
	dd′	−5.85	−8.65	−7.81	−5.57	−8.35	−9.26	5.91
	Mean ± SD							4.86 ± 1.08
4	aa′	−3.91	−2.44	−7.32	−3.61	−2.48	−6.54	2.12
	bb′	−4.4	−2.46	−8.3	−4.97	−4.02	−8.67	7.46
	cc′	−4.84	−3.92	−13.25	−5.23	−5.52	−11.94	8.16
	dd′	−5.37	−3.97	−10.74	−5.37	−3.87	−11.9	2.81
	Mean ± SD							5.14 ± 3.11
5	aa′	−3.88	−5.07	−8.31	−3.99	−5.95	−8.5	3.43
	bb′	−3.41	−3.77	−8.59	−4.92	−3.28	−7.42	11.26
	cc′	−4.88	−5.01	−10.23	−3.92	−5.47	−10.07	4.86
	dd′	−3.9	−3.9	−8.78	−5.12	−4.38	−8.5	6.77
	Mean ± SD							6.58 ± 3.41
Total	Mean ± SD							5.34 ± 2.48

Abbreviations: No. = number; exp. = experimental group; aa′, bb′, cc′, dd′ = vector quantity; A.E. = angle error; SD = standard deviation.

Table 2b
Angle error for system in the control group.

No. of ctrl. patients		Virtue			Reality			A.E. (°)
		X1	Y1	Z1	X2	Y2	Z2	
1	aa′	−0.97	−5.04	7.81	−3.42	−6.25	8.3	12.91
	bb′	−1.47	−5.13	8.79	−2.44	−6.26	8.69	7.11
	cc′	−1.95	−6.22	11.23	−2.93	−8.68	10.26	11.65
	dd′	−2.44	−6.08	11.23	−0.49	−7.51	11.23	10.22
	Mean ± SD							10.47 ± 2.50
2	aa′	−4.39	−3.79	6.35	−3.42	−5.06	6.83	10.15
	bb′	−3.91	−3.68	5.38	−7.33	−5.03	5.91	13.30
	cc′	−4.88	−5.11	6.84	−3.9	−5.01	7.32	6.38
	dd′	−5.37	−5.22	6.84	−7.33	−7.36	5.86	13.00
	Mean ± SD							10.71 ± 3.21
3	aa′	−5.37	−7.43	7.32	−4.88	−4.96	7.51	10.66
	bb′	−5.37	−7.49	7.32	−7.32	−6.33	6.34	12.12
	cc′	−5.86	−8.66	7.32	−5.86	−8.8	8.79	4.76
	dd′	−4.88	−7.45	7.33	−5.86	−7.2	8.3	5.06
	Mean ± SD							8.15 ± 3.79
4	aa′	−3.91	−1.2	9.28	−1.48	−1.31	7.82	12.28
	bb′	−3.91	−2.63	9.77	−6.83	−2.53	9.53	13.58
	cc′	−4.88	−2.72	10.74	−2.44	−2.39	11.72	12.51
	dd′	−3.9	−1.09	10.74	−6.35	−2.02	9.27	15.08
	Mean ± SD							13.36 ± 1.28
5	aa′	−7.81	−2.65	9.76	−8.72	−2.64	9.28	4.46
	bb′	−6.84	−2.46	8.79	−4.39	−1.38	9.74	14.35
	cc′	−7.81	−2.47	10.74	−10.26	−2.37	8.81	13.12
	dd′	−5.86	−2.35	7.32	−6.84	−1.5	8.79	6.45
	Mean ± SD							9.60 ± 4.88
Total	Mean ± SD							10.46 ± 3.46

Abbreviations: No. = number; ctrl. = control group; aa′, bb′, cc′, dd′ = vector quantity; A.E. = angle error; SD = standard deviation.

helpful in treating patients with prominent mandibular angles. In addition, our study provides a foundation for future clinical applications of MASO and other types of craniomaxillofacial surgery.

Financial support

Financial support was provided by National Natural Science Foundation of China (No. 81372097, No. 30600650, Nos. 61190124, 61190120), The Shanghai Committee of Science and Technology, China (No. 13DZ1108905, No. 13DZ1108900, No. 14441900800, Nos. 14441900802, YG2014MS06), National High Technology Research and Development Program of China (No. 2015AA043203), Project of SJTU Medical and Engineering Cross Fund (YJ2013ZD03).

Conflict of interests

The authors confirm that there are no known conflicts of interest associated with this publication.

Acknowledgments

This work was supported by National Natural Science Foundation of China (No. 81372097, No. 30600650, Nos. 61190124, 61190120), The Shanghai Committee of Science and Technology, China (No. 13DZ1108905, No. 13DZ1108900, No. 14441900800, Nos. 14441900802, YG2014MS06), National High Technology Research and Development Program of China (No. 2015AA043203), Project of SJTU Medical and Engineering Cross Fund (YJ2013ZD03).

References

Badiali G, Ferrari V, Cutolo F, Freschi C, Caramella D, Bianchi A, et al: Augmented reality as an aid in maxillofacial surgery: validation of a wearable system allowing maxillary repositioning. J Craniomaxillofac Surg 42(8): 1970–1976, 2014

Berryman DR: Augmented reality: a review. Med Ref Serv Q 31(2): 212–218, 2012

Cabrilo I, Bijlenga P, Schaller K: Augmented reality in the surgery of cerebral aneurysms: a technical report. Neurosurgery (Suppl. 2): 252–260, 2014 discussion 260-1

Deguchi M, Iio Y, Kobayashi K, Shirakabe T: Angle-splitting ostectomy for reducing the width of the lower face. Plast Reconstr Surg 99(7): 1831–1839, 1997

Hoffmann J, Westendorff C, Leitner C, Bartz D, Reinert S: Validation of 3D-laser surface registration for image-guided cranio-maxillofacial surgery. J Craniomaxillofac Surg 33(1): 13–18, 2005

Hong SO, Ohe JY, Lee DW: Salvage of the condylar fracture: complication management of mandibular angle ostectomy. J Craniofac Surg 25(6): e582–e584, 2014

Hughes-Hallett A, Mayer EK, Marcus HJ, Cundy TP, Pratt PJ, Darzi AW, et al: Augmented reality partial nephrectomy: examining the current status and future perspectives. Urology 83(2): 266–273, 2014

Kwoh YS, Hou J, Jonckheere EA, Hayati S: A robot with improved absolute positioning accuracy for CT guided stereotactic brain surgery. IEEE Trans Biomed Eng 35(2): 153–160, 1988

Marmulla R, Hoppe H, Muhling J, Eggers G: An augmented reality system for image-guided surgery. Int J Oral Maxillofac Surg 34(6): 594–596, 2005

Marzano E, Piardi T, Soler L, Diana M, Mutter D, Marescaux J, et al: Augmented reality-guided artery-first pancreatico-duodenectomy. J Gastrointest Surg 17(11): 1980–1983, 2013

Mischkowski RA, Zinser MJ, Kübler AC, Krug B, Seifert U, Zöller JE: Application of an augmented reality tool for maxillary positioning in orthognathic surgery—a feasibility study. J Craniomaxillofac Surg 34(8): 478–483, 2006

Park JL, Oh CH, Hwang K, Park CG: Burring and holes connecting ostectomy for the correction of prominent mandible angle. J Craniofac Surg 25: 1025–1027, 2014

Pugin F, Bucher P, Morel P: History of robotic surgery: from AESOP (R) and ZEUS (R) to da Vinci (R). J Visceral Surg 148(5 Suppl.): e3–e8, 2011

Qu M, Hou Y, Xu Y, Shen C, Zhu M, Xie L, et al: Precise positioning of an intraoral distractor using augmented reality in patients with hemifacial microsomia. J Craniomaxillofac Surg 43(1): 106–112, 2014

Selber JC: Robotics in plastic surgery. Semin Plast Surg 28(1): 3–4, 2014

Souzaki R, Ieiri S, Uemura M, Ohuchida K, Tomikawa M, Kinoshita Y: An augmented reality navigation system for pediatric oncologic surgery based on preoperative CT and MRI images. J Pediatr Surg 48(12): 2479–2483, 2013

Szabó Z, Berg S, Sjökvist S, Gustafsson T, Carleberg P, Uppsäll M, et al: Real-time intraoperative visualization of myocardial circulation using augmented reality temperature display. Int J Cardiovasc Imaging 29(2): 521–528, 2013

Tsuji M, Noguchi N, Shigematsu M, Yamashita Y, Ihara K, Shikimori M, et al: A new navigation system based on cephalograms and dental casts for oral and maxillofacial surgery. Int J Oral Maxillofac Surg 35(9): 828–836, 2006

Valero R, Ko YH, Chauhan S, Schatloff O, Sivaraman A, Coelho RF, et al: Robotic surgery: history and teaching impact. Actas Urol Esp 35(9): 540–545, 2011

Yang J, Wang L, Xu H, Tai N, Fan Z: Mandibular oblique ostectomy: an alternative procedure to reduce the width of the lower face. J Craniofac Surg 20(Suppl. 2): 1822–1826, 2009

Zemirline A, Agnus V, Soler L, Mathoulin CL, Liverneaux PA, Obdeijn M: Augmented reality-based navigation system for wrist arthroscopy: feasibility. J Wrist Surg 2(4): 294–298, 2013

Zhu M, Chai G, Zhang Y, Ma XF, Gan JL: Registration strategy using occlusal splint based on augmented reality for mandibular angle oblique split osteotomy. J Craniofac Surg 22(5): 1806–1809, 2011